Research Square

Preprints are preliminary reports that have not undergone peer review.
They should not be considered conclusive, used to inform clinical practice,
or referenced by the media as validated information.

Dynamic damage constitutive model for water-saturated and frozen sandstone after cyclic freeze-thaw treatment

Xin Xiong

xiuongxin@csu.edu.cn

Central South University

Feng Gao

Central South University

Keping Zhou

Central South University

Cong Li

Central South University

Research Article

Keywords: Damage constitutive model for rock, Freeze-thaw weathering treatment, Parameter sensitivity analysis, Dynamic compression, Split Hopkinson Pressure Bar

Posted Date: November 26th, 2026

DOI: https://doi.org/10.21203/rs.3.rs-11744899/v1

License: This work is licensed under a Creative Commons Attribution 4.0 International License.
Read Full License

Additional Declarations: No competing interests reported.

Dynamic damage constitutive model for water-saturated and frozen sandstone after cyclic freeze-thaw treatment

Xin Xiong*, Feng Gao, Keping Zhou, Cong Li

School of Resources and Safety Engineering, Central South University, Changsha, Hunan, 410083, PR China

* *Corresponding author*: xiuongxin@csu.edu.cn (Xin Xiong)

Abstract: The dynamic damage constitutive model of rock undergoing cyclic freeze-thaw is an important theoretical basis for analysing and predicting the deformation and strength characteristics of rock in cold regions, which has crucial practical and theoretical significance for guiding the numerical simulation, construction and operation of rock mass engineering in cold area environments. In this study, modified Split Hopkinson Pressure Bar (SHPB) was adopted to carry out dynamic compression tests on sandstone specimens experienced different numbers of freeze-thaw cycles. Experimental results indicate that under the condition of constant impact air pressure, the stress-strain curve of water-saturated sandstone gradually presents an obvious compaction stage with the increase of freeze-thaw cycles, while this compaction stage is not observed in frozen sandstone. On the contrary, with a fixed number of freeze-thaw cycles, the compaction stage in the stress-strain curve of water-saturated sandstone gradually reduces and even disappears as the impact air pressure rises, and the frozen sandstone still shows no compaction stage during the whole process. Based on the Z-W-T constitutive model, a dynamic damage constitutive model of freeze-thawed sandstone considering initial meso-damage, the number of freeze-thaw cycles and test states was established, and the model was verified by experimental data. The comparison results show that the established model can accurately characterize the dynamic compression deformation and strength properties of both water-saturated and frozen sandstone after cyclic freeze-thaw. In addition, sensitivity analysis of model parameters was carried out to further reveal the physical significance of each parameter.

Keywords: Damage constitutive model for rock; Freeze-thaw weathering treatment; Parameter sensitivity analysis; Dynamic compression; Split Hopkinson Pressure Bar.

1 Introduction

Rock constitutive model is a mathematical expression that describes the stress-strain relationship of rock under external loading, which can characterize the mechanical response behavior of rock and provide a theoretical basis for researchers to analyze and predict rock deformation and strength evolution. As a core research content in rock mechanics, it plays an irreplaceable role in engineering numerical simulation and practical construction application.(Wang et al. 2018). Therefore, the rock damage constitutive model has always been a research hotspot in the field of rock mechanics, and scholars have conducted in-depth and extensive research on it, and achieved abundant research results.(Bruning et al. 2019, Li et al. 2012, Shen et

al. 2019, Wang et al. 2021). However, due to the complexity of the rock and the different external environments (such as high and low temperatures(Ke et al. 2018, Miao et al. 2020, Rong et al. 2021, Weng et al. 2020), humidity(Liang et al. 2022, Ma et al. 2021), acid and alkali conditions(Huang et al. 2022, Lin et al. 2019), etc.), the mechanical properties and deformation laws of rock under external loading show significant differences under different working conditions. Thus, it is necessary to further explore and study the damage constitutive model of rock under different working conditions.

According to statistics, approximately 50% of the world's land area is distributed with seasonal frozen soil and permafrost regions (Liu et al. 2019). In these areas, due to diurnal and seasonal temperature variations, rocks frequently undergo freeze-thaw cycles resulting in continuous deterioration of the internal structure.(Momeni et al. 2015, Park et al. 2014). Under external loading, the mechanical response of freeze-thawed rock is quite different from those under conventional conditions. Using the rock damage constitutive model under conventional conditions to carry out engineering practice and numerical simulation may be different from the actual situation, and even threaten the safety of rock mass engineering in these areas. Therefore, it is of great engineering significance to carry out in-depth research on the damage constitutive model of freeze-thawed rock.

Based on the generalized strain equivalent theory, Fang et al. (2019) developed a damage statistical constitutive model of rock under freeze-thaw and uniaxial loading. Zhou et al. (2020) proposed a fractal damage constitutive model of freeze-thawed rock considering residual strength by using the fractal characteristics of rock section macroscopic images. Based on the internal state variable theory and thermodynamic principles Wang et al. (2019) constructed a stress-temperature-water coupled plastic incremental constitutive model for freeze-thawed rock. Qu et al. (2018) established a damage constitutive model of acidic freeze-thawed sandstone under loading by introducing a total damage correction coefficient, this model is characterized by its consideration of the influence of freeze-thaw cycles in acidic environment on the compaction stage of rock stress-strain curve. Gao et al. (2021) put forward a new piecewise constitutive model of rock under freeze-thaw and uniaxial loading, which could well describe the whole deformation process of sandstone including compaction, elastic deformation, yield and failure. Referring to the previous research results, Chen et al. (2022) divided the deformation of freeze-thaw rock in the compaction stage into the skeleton and void deformation, and a constitutive model that considers the influence of the freeze-thaw cycles on the non-linear deformation characteristics of rock in the compaction stage was established. Combined with the improved Harris distribution and damage mechanics, constructed a constitutive model of freeze-thawed rock in the post-compaction stage, and finally obtained a segmented constitutive model of

freeze-thawed rock under uniaxial compression. Based on the random exponential relationship between strain difference and strain in the compaction stage of frozen-thawed rock, Jiang et al. (2023) established a constitutive model considering the effect of freeze-thaw cycles on the nonlinear deformation of rock in the compaction stage, and combined with Weibull distribution and damage mechanics, established a constitutive model of the post-compaction stage, and further formed a segmented constitutive model of freeze-thawed rock under uniaxial compression. Huang et al. (2018) derived a statistical damage constitutive model of rock under freeze-thaw and triaxial loading, and applied it to the stability analysis of tunnels under thermo-hydro-mechanical coupling in cold regions. Lin et al. (2021) and Lu et al. (2019) established a damage constitutive models of freeze-thawed rock under triaxial loading based on Lognormal distribution and Weibull distribution, respectively. Based on the microcrack propagation and deformation law, Liu et al. (2021) constructed a constitutive model of freeze-thawed rock under triaxial loading. Zhang et al. (2020) and Shi et al. (2021) established damage constitutive models of freeze-thawed sandstone under triaxial loading considering the residual strength characteristics of sandstone. Based on the crack growth law and modified logistic equation, Zhang et al. (2021) and Meng et al. (2021) proposed constitutive models of freeze-thawed rock under triaxial loading respectively.

However, the above research results are all aimed at the static loading condition of freeze-thawed rock. In practical engineering, rock mass engineering often experiences dynamic loading(Liu et al. 2022, Wang et al. 2022), such as blasting, mechanical impact, and earthquake loading. Furthermore, in seasonal frozen soil regions, rock mass not only bears long-term cyclic freeze-thaw action caused by temperature changes, but also exists in frozen state in cold winter (with maximum temperatures below 0°C) and a water-saturated state in rainy summers. That is to say, the rock mass in seasonal frozen soil regions is mainly in two states: "freeze-thaw cycle (long-term) + frozen (short-term)" and "freeze-thaw cycle (long-term) + water-saturated (short-term)." Török et al. (2018) found that the strength and deformation behavior of rock with pore water or pore ice are quite different from those of dry rock, and the content of pore water and pore ice also has a significant impact on the mechanical properties of rock (Wang et al. 2023, Wang et al. 2021). Therefore, it is urgent to carry out in-depth research on the dynamic damage constitutive model for water-saturated and frozen rock after cyclic freeze-thaw treatment.

In this study, the sandstone was taken from the open-pit slope of the Jiama copper mine in Tibet, China. Firstly, the modified Split Hopkinson Pressure Bar (SHPB) was used to carry out dynamic compression mechanical tests on sandstone after being subjected to different numbers of freeze-thaw cycles. Secondly, based on the Z-W-T viscoelastic constitutive model, a dynamic damage constitutive model of freeze-thawed

sandstone considering initial meso-damage, freeze-thaw cycle times and different test states was established. Finally, the established dynamic constitutive model was verified by experimental data, and the sensitivity of model parameters was analyzed to reveal the influence law of each parameter on the model.

2 Experimental materials and methods

2.1 Rock specimen preparation

According to the rock dynamic mechanics test standard proposed by the ISRM (Ulusary 2014), and taking into account the relevant rock dynamic indoor test standards (Dai et al. 2010), the sandstone was processed into a cylindrical specimen with a diameter of 50 mm and a height of 50 mm. The flatness error of both end surfaces was controlled within 0.02 mm, and the vertical deviation was less than 0.001 radians. In order to reduce the dispersion of experimental results, sandstone specimens with large differences in longitudinal wave velocity and porosity were screened out after testing. A total of 40 qualified sandstone specimens were selected for dynamic compression tests, which were divided into 5 groups named CA, CB, CC, CD and CE, corresponding to 0, 10, 20, 30 and 40 freeze-thaw cycles respectively. Each group was further divided into 4 subgroups according to different impact air pressures (0.4 MPa, 0.5 MPa, 0.6 MPa and 0.7 MPa), and each subgroup contained two sandstone specimens for dynamic compression tests under water-saturated and frozen states respectively. The test scheme is detailed in Table 1.

Table 1 Specimen IDs for water-saturated (WSS) and frozen sandstone (FS)

Freeze-thaw cycles	Impact gas pressure/MPa			
/*n*	0.4	0.5	0.6	0.7
0	CA1 and CA3	CA5 and CA7	CA9 and CA11	CA13 and CA15
10	CB1 and CB3	CB5 and CB7	CB9 and CB11	CB13 and CB15
20	CC1 and CC3	CC5 and CC7	CC9 and CC11	CC13 and CC15
30	CD1 and CD3	CD5 and CD7	CD9 and CD11	CD13 and CD15
40	CE1 and CE3	CE5 and CE7	CE9 and CE11	CE13 and CE15

Note: The specimen numbers with odd digits 1,5,9,13 represent water-saturated sandstone, and 3,7,11,15 represent frozen sandstone.

2.2 Test process

The dynamic compression tests of WSS and FS in group CA (0 freeze-thaw cycles) were carried out directly, while the specimens in other groups were subjected to cyclic freeze-thaw tests first and then dynamic compression tests. The experimental procedure is as follows:

(1) All sandstone specimens were dried to constant weight in an oven, and then numbered and grouped according to the test scheme after cooling to room temperature.

(2) All specimens in group CA were subjected to vacuum water saturation treatment. After saturation, the specimens numbered 1,5,9,13 were directly used for dynamic compression tests under water-saturated state; the specimens numbered 3,7,11,15 were gently wiped to remove surface water, wrapped with plastic

wrap and placed in a low-temperature test chamber for freezing at -20° C for 48 h (to ensure complete freezing of the specimens). After freezing, the plastic wrap was removed, and Vaseline was evenly coated on the end faces of the incident bar, transmission bar and rock specimens to eliminate the end effect, and then dynamic compression tests under frozen state were carried out.

(3) The cyclic freeze-thaw tests of specimens in groups CB, CC, CD and CE were carried out by using a TDS-300 freeze-thaw cycle testing machine. All specimens were placed in the freeze-thaw test box, the freezing temperature was set to -20° C, the thawing temperature was set to 20° C, and each freeze-thaw cycle included 4 h of freezing and 4 h of thawing. The temperature change curve during the freeze-thaw cycle is shown in Fig. 1.

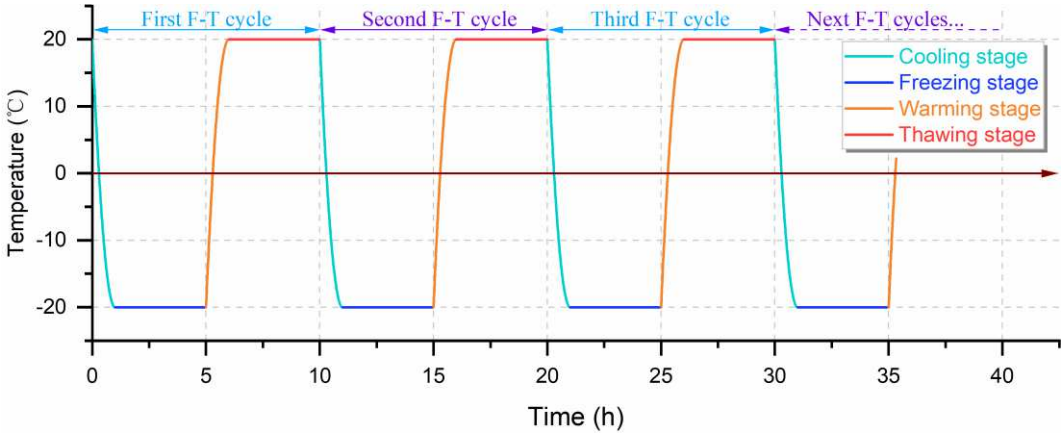

Fig. 1 The temperature change curve of the freeze-thaw cycle

(4) When the specimens in groups CB, CC, CD and CE reached the preset freeze-thaw cycles (10, 20, 30 and 40 times respectively), they were taken out from the freeze-thaw test box, and the dynamic compression tests under water-saturated and frozen states were carried out by repeating the operation steps in (2). The whole experimental flow is shown in Fig. 2.

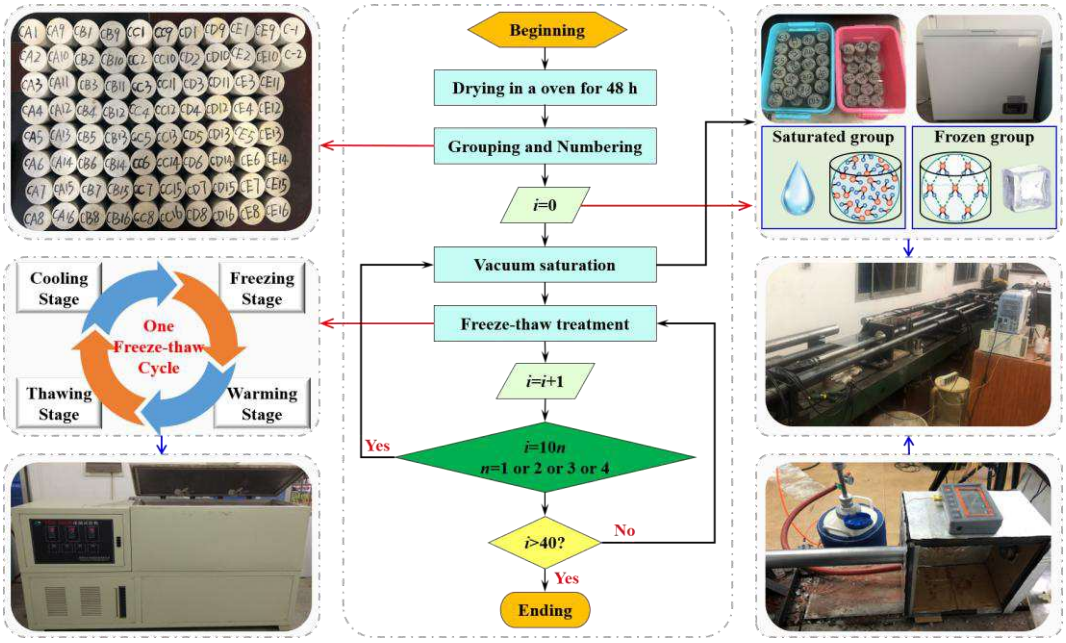

Fig. 2 Experimental procedure

2.3 Split Hopkinson Pressure Bar test

The dynamic compression tests were carried out by using the SHPB test system of Central South University(Li et al. 2004). The incident bar, transmission bar and spindle-shaped striker of the test system were all made of 40Cr alloy steel with a density of 7810 kg·m^{-3}. The data acquisition is completed by strain gauges on the incident and transmission bars, ultra-dynamic strain gauges, oscilloscopes, and computers. In order to study the dynamic mechanical behavior of rock under frozen state, the original SHPB test system was modified to eliminate the influence of room temperature. The low-temperature environment box was added to control the rock specimens in the frozen state during dynamic loading. The low-temperature environmental box was built on the SHPB platform. The main structure of the environmental box is plexiglass with good air tightness, and the inner and outer walls of the plexiglass were pasted with insulation material. At the bottom and top of the box, there is a stainless-steel pipe connecting the inside of the box. The valve of the pipe can control the entry and exit of low-temperature nitrogen. Circular holes with a diameter slightly larger than 50 mm were reserved on both sides of the box for the passage of incident bar and transmission bar, and thermal insulation materials were wrapped around the holes to ensure the low-temperature environment inside the box. A sliding door was set on the front of the box to facilitate the placement and taking out of rock specimens. A thermocouple was installed inside the box to monitor the temperature in real time, and the temperature control switch could automatically adjust the input of low-temperature nitrogen according to the thermocouple monitoring data, with a temperature control accuracy of 0.1℃. The schematic diagram of the modified SHPB test system with low-temperature control function is shown in Fig. 3.

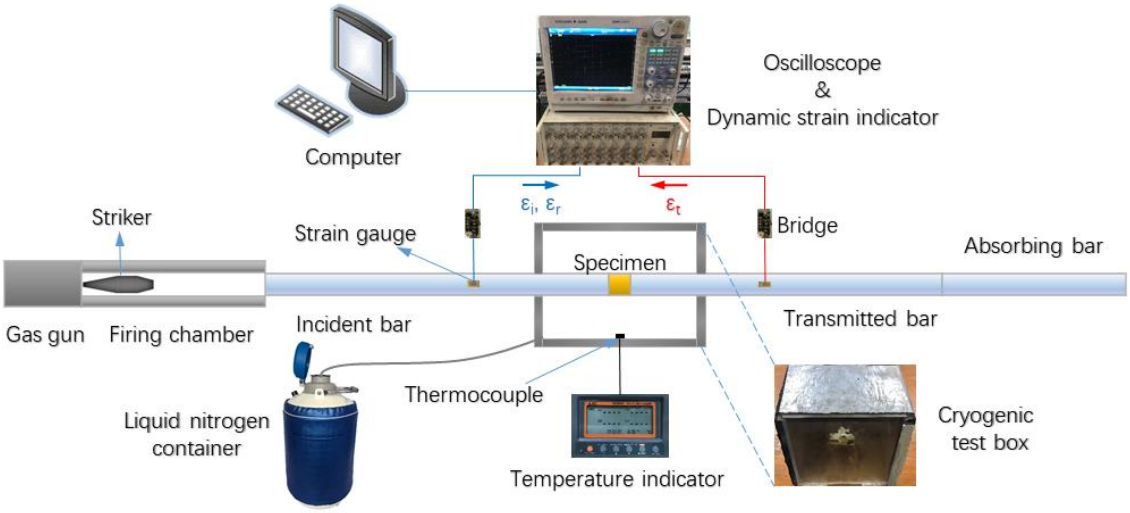

Fig. 3 Schematic of the SHPB test system with cryogenic control

2.4 Stress equilibrium

In this test, a spindle-shaped striker was used to generate a half-sine incident wave, which could ensure that the sandstone specimens were loaded at a relatively constant strain rate. For the SHPB dynamic

compression test to be effective, the basic requirement is that the rock specimens reach the stress equilibrium state before failure.

Taking specimen CA1 as an example, Fig. 4a shows the original strain signals collected by the ultra-dynamic strain gauge from the strain gauges on the incident bar and transmission bar, and Fig. 4b shows the stress equilibrium verification curve of CA1 after data processing, which is composed of incident wave, reflected wave and transmitted wave. It can be seen from Fig. 4b that the superposition curve of incident wave and reflected wave is basically consistent with the transmitted wave curve, which indicates that specimen CA1 has reached the stress equilibrium state during the loading process. In this study, the stress equilibrium of all freeze-thawed sandstone specimens used for dynamic compression tests was strictly verified, and only the specimens that met the stress equilibrium requirements were selected for subsequent data analysis.

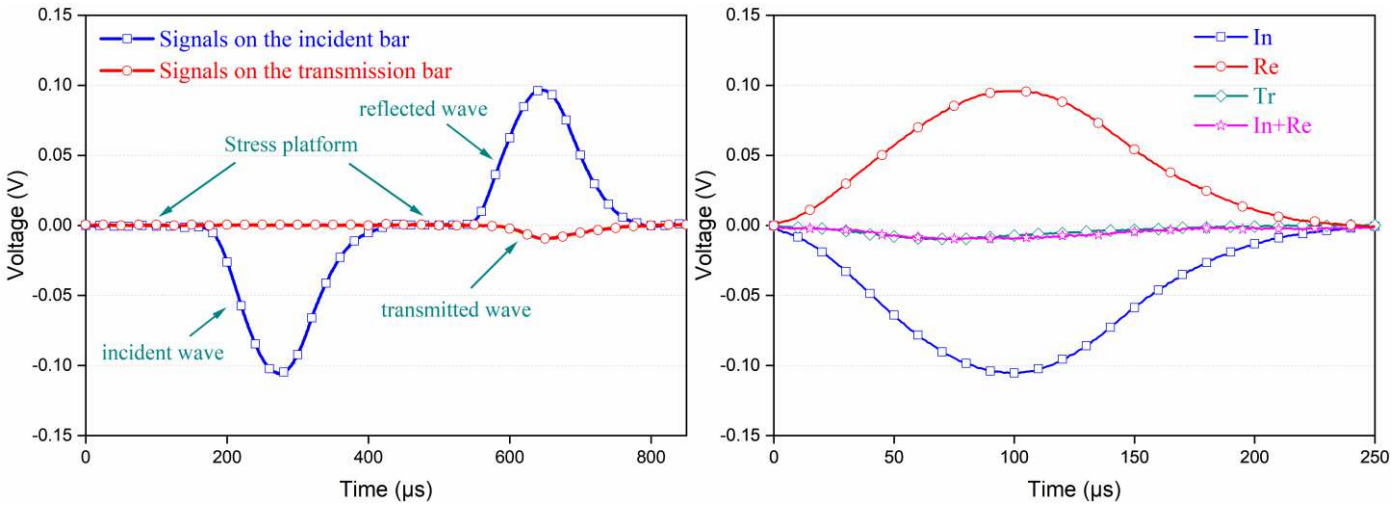

(a) Signals on the bars **(b) Signals reach stress equilibrium**

Fig. 4 Stress equilibrium

In the SHPB dynamic compression test, the striker is driven by high-pressure gas to impact the incident bar, and an incident stress wave is generated in the incident bar and propagates to the rock specimen at the interface of incident bar-specimen-transmission bar. Due to the difference in material properties, a part of the incident wave is reflected back to the incident bar to form a reflected wave, and the other part passes through the specimen to the transmission bar to form a transmitted wave. The SHPB test is based on the assumption of one-dimensional stress wave, which means that only the axial deformation of the stress wave during propagation is considered, and the radial deformation is ignored. Based on the one-dimensional stress wave assumption and taking the dynamic loading direction as the positive direction, the strain, strain rate and stress calculation formulas of the specimen are derived as follows (Li et al. 2008):

$$\varepsilon = \frac{u_1 - u_2}{H_s} = \frac{C_e}{H_s}\int_0^t (\varepsilon_i - \varepsilon_r - \varepsilon_t)dt \tag{1}$$

$$\dot{\varepsilon} = \frac{d\varepsilon}{dt} = \frac{C_e}{H_s}(\varepsilon_i - \varepsilon_r - \varepsilon_t) \quad (2)$$

$$\sigma_c = \frac{P_1 + P_2}{2A_s} = \frac{A_e E_e}{2A_s}(\varepsilon_i + \varepsilon_r + \varepsilon_t) \quad (3)$$

where ε, $\dot{\varepsilon}$ and σ are the strain, strain rate, and stress of the specimen, respectively; u_1 and u_2 are the axial displacements of the incident bar and transmission bar at the specimen interface, respectively; A_e, C_e and E_e denote the cross-sectional area, longitudinal wave velocity, and elastic modulus of the SHPB bars, respectively; P_1 and P_2 are the dynamic forces acting on the two end faces of the rock specimen; and L_s and A_s are the length and cross-sectional area of the rock specimen respectively.

According to the test collected signal data, the dynamic compressive strength and corresponding strain rate of WSS and FS after different freeze-thaw cycles under different impact pressures were calculated by using the above formulas, and the test results are shown in Table 2.

Table 2 Dynamic compressive strength and corresponding strain rate of WSS and FS

Water-saturated group			Frozen group		
Specimen ID	Strain rate / s^{-1}	Dynamic compressive strength/MPa	Specimen ID	Strain rate /s^{-1}	Dynamic compressive strength/MPa
CA1	82.2	47.904	CA3	91.2	57.836
CA5	101.1	51.371	CA7	108.7	62.204
CA9	121.4	57.154	CA11	130.4	67.485
CA13	147.6	62.175	CA15	156.5	72.885
CB1	84.0	44.043	CB3	92.4	60.764
CB5	103.9	47.826	CB7	110.7	65.349
CB9	124.2	50.896	CB11	132.2	70.790
CB13	149.5	55.661	CB15	157.6	76.782
CC1	86.2	40.588	CC3	94.1	63.141
CC5	105.1	43.742	CC7	111.8	68.595
CC9	126.0	46.075	CC11	133.9	73.967
CC13	151.5	49.311	CC15	159.2	81.638
CD1	88.5	37.650	CD3	95.9	65.709
CD5	107.6	39.733	CD7	113.1	71.140
CD9	127.5	42.877	CD11	135.3	77.921
CD13	152.6	45.909	CD15	160.8	86.069
CE1	90.1	34.426	CE3	97.3	68.702
CE5	108.2	36.267	CE7	114.5	74.379
CE9	129.8	38.027	CE11	136.5	82.111
CE13	154.9	40.976	CE15	162.2	90.339

3 Establishment of a dynamic constitutive model for frozen-thawed sandstone

3.1 Dynamic constitutive model based on initial damage

The combined constitutive models commonly used in rock mechanics can be divided into two categories: viscoelastic and viscoelastic-plastic constitutive model. In the viscoelastic constitutive model, it is generally

considered that the material is composed of a pure viscous body and a pure elastic body. The material is regarded as two heterogeneous particles, different types of viscoelastic materials are described by different combinations of two kinds of particles or different combinations of the element, such as Maxwell body, Burgers body, and Kelvin body. In the viscoelastic-plastic constitutive model, the influence of viscosity, elasticity, and plasticity of the material on its mechanical behavior is considered. In addition to the heterogeneous pure viscous body and pure elastic body, a non-pure plastic body is also added. Different types of viscoelastic-plastic materials are described by different combinations of these three particles or different combinations of the element. Due to the introduction of the non-pure plastic body, the viscoelastic-plastic model is more widely used than the viscoelastic model. However, in practical application and research, the viscoelastic-plastic model mainly studies the relationship between stress, strain, and time when the stress is greater than the yield limit of the material, and the viscoelastic model mainly studies the relationship between stress, strain, and time when the stress is less than the yield limit of the material. The dynamic behavior of frozen-thawed sandstone presents the characteristics of viscosity, elasticity, and plasticity, but for the brittle material of rock mass, the plastic behavior is very weak and negligible, and there is no yield stage in the dynamic stress-strain curve. After comprehensive consideration, a typical series-parallel combined viscoelastic model is selected, and a mesoscopic damage characterization method is introduced to better reflect the dynamic mechanical properties of frozen-thawed sandstone.

In this study, the Z-W-T constitutive model was adopted to characterize the dynamic damage behavior of freeze-thawed sandstone. The model is a nonlinear viscoelastic constitutive model established by Green and Rivlin based on a large number of impact dynamic test data of polymer viscoelastic materials, and a large number of studies have shown that this model can well simulate the strength and deformation characteristics of brittle materials such as sandstone under high strain rate loading, and can be used to characterize the coupling effect of cyclic freeze-thaw and dynamic loading on rock mechanical properties (Ma et al. 2017). The Z-W-T constitutive model is composed of a nonlinear spring and two Maxwell models in parallel, and its mathematical expression is shown in Eq. (4) and the combination of elements is shown in Fig. 5.

$$\sigma = E_0\varepsilon + \alpha\varepsilon^2 + \beta\varepsilon^3 + E_1\int_0^t \dot{\varepsilon}\exp\left(-\frac{t-\tau}{\theta_1}\right)d\tau + E_2\int_0^t \dot{\varepsilon}\exp\left(-\frac{t-\tau}{\theta_2}\right)d\tau \quad (4)$$

where the first three items are used to describe the nonlinear elastic response characteristics of the material, and he last two terms are the low-frequency and high-frequency Maxwell models respectively, which characterize the viscoelastic response of the material. E_0, α and β are the elastic constants corresponding

to the nonlinear elastic equilibrium response of the material, E_1, θ_1, E_2 and θ_2 are the elastic modulus and relaxation time of the low-frequency and high-frequency Maxwell models respectively.

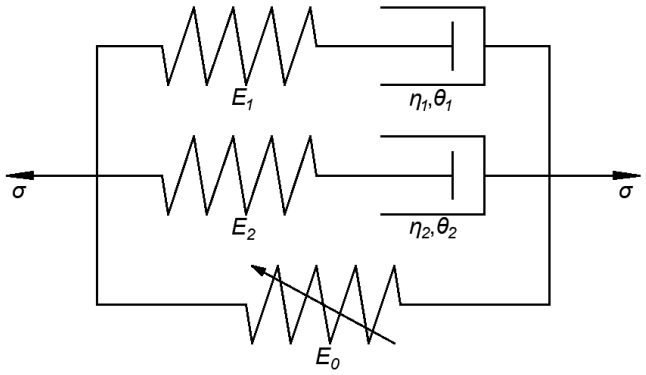

Fig. 5 The combination of elements for the Z-W-T constitutive model

In the Z-W-T constitutive model, the low-frequency and high-frequency Maxwell models are used to describe the viscoelastic response of materials under different strain rates respectively, among which the relaxation time θ_1 of the low-frequency Maxwell model is at the level of 10^1~10^2s, while θ_2 only plays a role in the order of 10^{-4}~10^{-6}s. Based on the research of Zhang et al. (2020), under high strain rate loading, the microcracks in the rock specimen propagate and interact rapidly, and the low-frequency Maxwell model has no enough time to produce relaxation response, so its effect can be neglected. Therefore, Eq. (6) can be re-written as follows:

$$\sigma = E_0\varepsilon + \alpha\varepsilon^2 + \beta\varepsilon^3 + E_2\int_0^t \dot{\varepsilon}\exp\left(-\frac{t-\tau}{\theta_2}\right)d\tau \tag{5}$$

In addition, the Z-W-T constitutive model only contains elastic elements and viscous elements and does not consider the effect of mesoscopic damage on the constitutive relationship of freeze-thawed sandstone. Therefore, it is necessary to further improve the model and establish a dynamic damage constitutive model suitable for freeze-thawed sandstone by introducing the damage variable. The basic assumptions of the model improvement are as follows:

(1) The micro-elements of sandstone have both viscoelastic and damage characteristics; according to the mechanical characteristics of basic elements, the viscous element has no damage characteristics, so the elastic elements in the simplified Z-W-T model are replaced by damaged elastic elements $D_i(i = 0, 2)$ to modify the model.

(2) The distribution of micropores and microcracks in sandstone is isotropic, and the strength of the damaged elastic micro-elements obeys the Weibull distribution (Tang 1997), and its probability density function is:

$$\psi(\varepsilon) = \frac{m}{\gamma}\varepsilon^{m-1}\exp\left[-\left(\frac{\varepsilon}{\gamma}\right)^m\right] \tag{6}$$

where m and γ are the shape parameter and scale parameter of Weibull distribution respectively, which are related to the material properties and meso-structure of rock.

The damage degree of sandstone is determined by the number and size of micropores and microcracks in the micro-elements, which directly affects the strength of the micro-elements. The damage variable D is introduced to characterize the damage degree of sandstone, and its relationship with the failure probability density of micro-elements is:

$$\frac{dD}{d\varepsilon} = \psi(\varepsilon) \tag{7}$$

Integrating Eq. (7), the expression of the damage variable can be obtained:

$$D = 1 - \exp\left[-\left(\frac{\varepsilon}{\gamma}\right)^m\right] \tag{8}$$

The elastic modulus of the damaged elastic element $D_i(i = 0, 2)$ is denoted as $\tilde{E}_i(i = 0, 2)$, According to the definition of damage variable, the relationship between the damaged elastic modulus and the intact elastic modulus is:

$$\tilde{E}_i = E_i(1 - D) = E_i\exp\left[-\left(\frac{\varepsilon}{\gamma}\right)^m\right] \tag{9}$$

Based on the above assumptions, the improved dynamic damage constitutive model is composed of damaged elastic element D_0, damaged elastic element D_2 and viscous element η_2 in series in parallel. The simplified Z-W-T constitutive model with elastic elements replaced by damaged elastic elements is shown in Fig. 6.

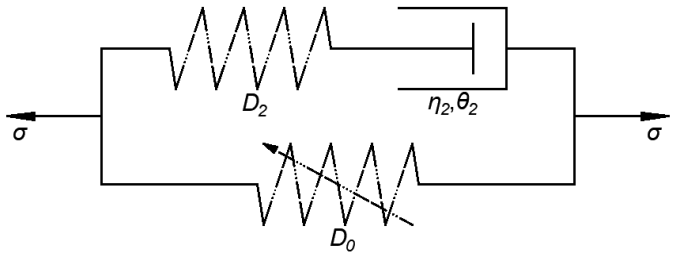

Fig. 6 The simplified Z-W-T constitutive model of the damaged body replacing the elastic body

According to Lemaitre's strain equivalence principle (Lemaitre 1996), the strain generated by the nominal stress acting on the damaged material is equivalent to the strain generated by the effective stress acting on the intact material with the same geometric size, and its mathematical expression is:

$$\varepsilon = \frac{\bar{\sigma}}{E} = \frac{\sigma}{E(1 - D)} = \frac{\sigma}{\tilde{E}} \tag{10}$$

where $\bar{\sigma}$ and σ are the effective stress and nominal stress, respectively. E and $\tilde{E}$ are the elastic modulus of the intact and damaged material respectively. D is the damage variable.

For the simplified Z-W-T constitutive model in Fig. 6:

①：Damaged elastic element D_0

Combined with Eq. (5), the damaged elastic element D_0 has the following relationship:

$$\sigma_0(t) = \tilde{E}_0\varepsilon + \tilde{\alpha}\varepsilon^2 + \tilde{\beta}\varepsilon^3 \tag{11}$$

Combined with Eqs. (9), (10), and (11), the constitutive relationship of damaged elastic element D_0 as follow:

$$\sigma_0(t) = (E_0\varepsilon_0 + \alpha\varepsilon_0^2 + \beta\varepsilon_0^3)\exp\left[-\left(\frac{\varepsilon_0}{\gamma_0}\right)^{m_0}\right] \tag{12}$$

②：Damaged elastic element D_2 is connected in series with the viscous element η_2

Combined with Eq. (5), the damaged elastic element D_2 is connected in series with the viscous element η_2 has the following relationship:

$$\sigma_2(t) = \tilde{E}_2\int_0^t \dot{\varepsilon}\exp\left(-\frac{t-\tau}{\theta_2}\right)d\tau \tag{13}$$

Combined with Eqs. (9), (10), and (13), the constitutive relationship of the damaged elastic element D_2 is connected in series with the viscosity viscous element η_2 as follow:

$$\sigma_2(t) = E_2\exp\left[-\left(\frac{\varepsilon_2}{\gamma_2}\right)^{m_2}\right]\int_0^t \dot{\varepsilon}_2\exp\left(-\frac{t-\tau}{\theta_2}\right)d\tau \tag{14}$$

In the dynamic impact test, the loading rate is extremely fast, and Eq. (14) is simplified to constant strain rate loading, Eq. (14) can be re-written as:

$$\sigma_2(t) = E_2\dot{\varepsilon}_2\theta_2\exp\left[-\left(\frac{\varepsilon_2}{\gamma_2}\right)^{m_2}\right]\left[1-\exp\left(-\frac{\varepsilon_2}{\dot{\varepsilon}_2\theta_2}\right)\right] \tag{15}$$

③：① and ② in parallel

According to the basic principle of parallel mechanical elements:

$$\sigma(t) = \sigma_0(t) + \sigma_2(t) \tag{16}$$

$$\varepsilon(t) = \varepsilon_0(t) = \varepsilon_2(t) \tag{17}$$

Combined with Eqs. (12), (15), (16), and (17), the dynamic damage constitutive model of sandstone considering initial meso-damage can be obtained:

$$\sigma = \begin{cases} (E_0\varepsilon + \alpha\varepsilon^2 + \beta\varepsilon^3)\exp\left[-\left(\dfrac{\varepsilon}{\gamma_0}\right)^{m_0}\right] \\ +E_2\dot{\varepsilon}\theta_2\exp\left[-\left(\dfrac{\varepsilon}{\gamma_2}\right)^{m_2}\right]\left[1-\exp\left(-\dfrac{\varepsilon}{\dot{\varepsilon}\theta_2}\right)\right] \end{cases} \tag{18}$$

where E_0, α and β are the elastic constants of the nonlinear elastic equilibrium response; m_0, m_2, γ_0, and γ_2 are the Weibull distribution parameters. θ_2 is the relaxation time of the high-frequency Maxwell model, which characterizes the dynamic response time of the material under high strain rate loading.

3.2 Dynamic constitutive model considering F-T cycles

Rock mass in seasonal frozen regions is continuously subjected to cyclic freeze-thaw action due to temperature changes, which leads to the accumulation of freeze-thaw damage and the deterioration of mechanical properties. The above dynamic damage constitutive model only considers the initial meso-damage of sandstone, and does not take into account the influence of cyclic freeze-thaw action on the dynamic mechanical behavior of sandstone, so it cannot fully reflect the mechanical response characteristics of freeze-thawed sandstone in cold regions. Therefore, it is necessary to introduce the freeze-thaw cycle influence factor to modify the model and establish a dynamic damage constitutive model considering the number of freeze-thaw cycles and test states.

Referring to the research results of Gao et al.(2022), an exponential model with attenuation and strengthening factors was introduced to characterize the influence of cyclic freeze-thaw on the dynamic compressive strength of sandstone, and its mathematical expression is:

$$\frac{\sigma_{c,S,(n)}}{\sigma_{c,S,(0)}} = e^{-\lambda_a(\dot{\varepsilon})n} \tag{19}$$

$$\frac{\sigma_{c,F,(n)}}{\sigma_{c,F,(0)}} = e^{\lambda_i(\dot{\varepsilon})n} \tag{20}$$

where λ_a and λ_i are the strength attenuation factor of water-saturated sandstone and strength strengthening factor of frozen sandstone under cyclic freeze-thaw respectively, which are related to the strain rate; n is the number of freeze-thaw cycles; $\sigma_{c,S,(n)}$ and $\sigma_{c,S,(0)}$ are the dynamic compressive strengths of water-saturated sandstone after *n* freeze-thaw cycles and before freeze-thaw cycles, respectively; and $\sigma_{c,F,(n)}$ and $\sigma_{c,F,(0)}$ are the dynamic compressive strengths of frozen sandstone after *n* freeze-thaw cycles and before freeze-thaw cycles, respectively.

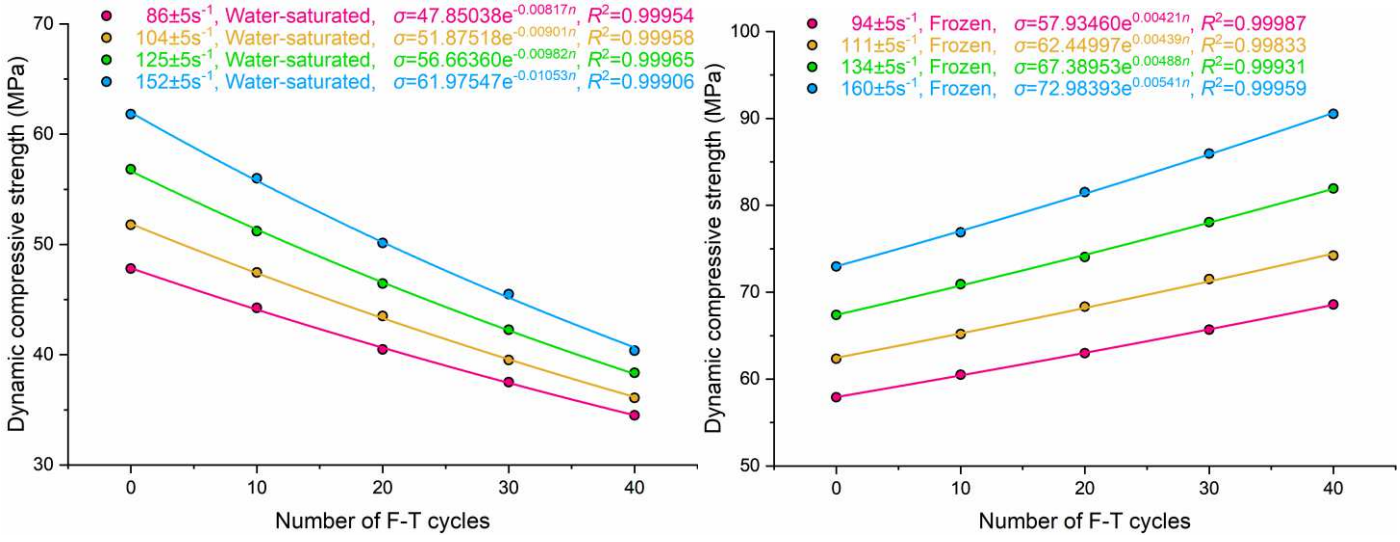

(a) Water-saturated specimens **(b) Frozen specimens**

Fig. 7 Relationship between dynamic compressive strength and the number of F-T cycles

Fig. 7 shows the relationship between the dynamic compressive strength of sandstone and the number of freeze-thaw cycles. It can be seen from the figure that with the increase of freeze-thaw cycle times, the

dynamic compressive strength of water-saturated sandstone shows an exponential attenuation trend, while the dynamic compressive strength of frozen sandstone shows an exponential growth trend. Based on this, the freeze-thaw cycle influence index K_c is introduced to characterize the influence of cyclic freeze-thaw on the strength of sandstone, and its calculation formula is:

$$K_c = ln\left[\frac{\sigma_n}{\sigma_0}\right]/n \tag{21}$$

where K_c is the freeze-thaw cycle influence index, when the test state is water-saturated, its value is $-\lambda_a$, and when the test state is frozen, its value is λ_i. σ_n and $\sigma_0$are the dynamic compressive strengths of water-saturated or frozen sandstone after *n* freeze-thaw cycles and before freeze-thaw cycles, respectively.

According to Eq. (21), σ_n can be re-written as follow:

$$\sigma_n = \sigma_0 e^{nK_c} \tag{22}$$

Taking Eq. (22) into Eq. (18), the dynamic damage constitutive model of sandstone considering the initial meso-damage, freeze-thaw cycle times and test states can be obtained:

$$\sigma_{(n)} = e^{nK_c}\left\{\begin{array}{c}(E_0\varepsilon + \alpha\varepsilon^2 + \beta\varepsilon^3)\exp\left[-\left(\frac{\varepsilon}{\gamma_0}\right)^{m_0}\right] \\ +E_2\dot{\varepsilon}\theta_2\exp\left[-\left(\frac{\varepsilon}{\gamma_2}\right)^{m_2}\right]\left[1-\exp\left(-\frac{\varepsilon}{\dot{\varepsilon}\theta_2}\right)\right]\end{array}\right\} \tag{23}$$

4 Verification and analysis of the dynamic constitutive model of frozen-thawed sandstone

4.1 Validation of the dynamic constitutive model

There are 11 parameters in the dynamic damage constitutive model of Eq. (23). The determination method is as follows: *n* is the number of freeze-thaw cycles and the value of K_c can be determined according to Eq. (21). At the corresponding strain rate, $\dot{\varepsilon}$ is a fixed value, and θ_2 is the dynamic response time. Here, the difference in the dynamic response time for different specimens can be ignored, and 250μs is taken uniformly. Because $\dot{\varepsilon}\theta_2$ always appears at the same time, it is bound as a whole for assignment. Therefore, there are 8 undetermined parameters in the model , which are E_0, E_2, α, β, γ_0, γ_2, m_0, and m_2, and these parameters can be obtained by fitting the experimental stress-strain data.

The experimental data of WSS and FS after different freeze-thaw cycles were used to fit and verify the established dynamic constitutive model, and the fitting parameters of the model are shown in Table 3. The comparison between the experimental stress-strain curve and the model theoretical curve of WSS and FS is shown in Fig. 8 and Fig. 9 respectively.

It can be seen from Fig. 8 that the theoretical curve of the model is in good agreement with the experimental stress-strain curve of water-saturated sandstone, and the main deformation stages (compaction, elastic, failure) can be well characterized, except for individual specimens with a small deviation between the

359 model curve and the experimental curve. This indicates that the established dynamic damage constitutive
360 model can accurately reflect the dynamic compression deformation and strength characteristics of water-
361 saturated sandstone after cyclic freeze-thaw.

362 **Table 3 Constitutive model parameters of WSS and FS under different freeze-thaw cycles**

Label	n	K_c	E_0	α	β	γ_0	m_0	E_2	$\dot{\varepsilon}\theta_2$	γ_2	m_2
CA1	0	-0.00817	1920	43000	12.9×10^7	0.0076	2.34	20700	20550	0.0040	1.21
CB1	10	-0.00817	1980	42000	12.1×10^7	0.0076	2.33	20900	21000	0.0040	1.22
CC1	20	-0.00817	2030	43000	13.3×10^7	0.0074	2.81	20200	21550	0.0040	1.29
CD1	30	-0.00817	2130	45000	10.3×10^7	0.0072	2.95	20400	22125	0.0040	0.98
CE1	40	-0.00817	3310	501000	9.6×10^7	0.0069	2.74	3900	22525	0.0149	1.21
CA5	0	-0.00901	1520	32000	9.5×10^7	0.0082	1.94	24900	25275	0.0040	1.05
CB5	10	-0.00901	1550	34000	9.4×10^7	0.0082	1.94	26100	25975	0.0040	1.02
CC5	20	-0.00901	1650	35000	9.2×10^7	0.0072	2.20	26000	26275	0.0041	1.01
CD5	30	-0.00901	1640	35000	9.4×10^7	0.0080	1.97	23900	26900	0.0041	1.01
CE5	40	-0.00901	4910	801000	8.4×10^7	0.0064	1.75	5500	27050	0.0107	1.01
CA9	0	-0.00982	1370	17000	9.4×10^7	0.0073	1.58	32200	30350	0.0040	1.02
CB9	10	-0.00982	1380	16000	9.4×10^7	0.0073	1.58	31200	31050	0.0040	1.02
CC9	20	-0.00982	1410	16000	9.4×10^7	0.0073	1.58	31300	31500	0.0040	1.02
CD9	30	-0.00982	1950	16000	12.4×10^7	0.0069	1.52	27800	31875	0.0041	0.98
CE9	40	-0.00982	7740	202000	12.7×10^7	0.0061	1.81	7300	32450	0.0099	1.23
CA13	0	-0.01053	1150	14000	9.3×10^7	0.0082	1.73	35900	36900	0.0040	1.09
CB13	10	-0.01053	1140	13000	8.8×10^7	0.0082	1.91	35500	37375	0.0040	1.09
CC13	20	-0.01053	1080	14000	8.8×10^7	0.0084	1.87	34900	37875	0.0040	1.09
CD13	30	-0.01053	1070	15000	8.9×10^7	0.0090	1.91	34600	38150	0.0040	1.03
CE13	40	-0.01053	9800	130000	8.5×10^7	0.0067	1.45	8800	38725	0.0079	1.06
CA3	0	000421	3440	146000	11.4×10^7	0.0080	2.97	21700	22800	00037	1.08
CB3	10	000421	3670	148000	11.8×10^7	0.0074	2.98	23500	23100	0.0037	1.04
CC3	20	000421	3580	148000	10.9×10^7	0.0073	2.99	24400	23525	0.0039	1.04
CD3	30	000421	3730	147000	11.3×10^7	0.0073	2.72	25100	23975	0.0037	1.07
CE3	40	000421	3870	144000	9.8×10^7	0.0073	2.53	26600	24325	0.0037	1.06
CA7	0	0.00439	3540	127000	9.6×10^7	0.0084	2.01	29900	27175	0.0037	1.07
CB7	10	0.00439	3620	137000	9.9×10^7	0.0084	1.89	30400	27675	0.0037	1.09
CC7	20	0.00439	3650	148000	9.6×10^7	0.0084	1.99	30500	27950	0.0037	1.09
CD7	30	0.00439	3640	142000	9.5×10^7	0.0084	1.97	30100	28275	0.0037	1.07
CE7	40	0.00439	3680	147000	9.3×10^7	0.0084	1.96	30200	28625	0.0037	1.07
CA11	0	0.00488	3720	98000	7.1×10^7	0.0093	2.35	33800	32600	0.0037	1.07
CB11	10	0.00488	3690	121000	7.3×10^7	0.0093	2.49	32900	33050	0.0038	1.18
CC11	20	0.00488	3790	96000	7.3×10^7	0.0093	2.33	33900	33475	0.0037	1.12
CD11	30	0.00488	3740	102000	7.7×10^7	0.0094	1.99	33700	33825	0.0038	1.15
CE11	40	0.00488	3750	103000	7.7×10^7	0.0095	1.99	33500	34125	0.0038	1.10
CA15	0	0.00541	3820	137000	6.9×10^7	0.0087	1.90	38200	39125	0.0037	0.98
CB15	10	0.00541	3720	136000	6.8×10^7	0.0087	1.89	38800	39400	0.0037	0.99
CC15	20	0.00541	3740	139000	6.9×10^7	0.0086	1.80	39700	39800	0.0037	1.01
CD15	30	0.00541	3670	135000	6.9×10^7	0.0087	1.81	40200	40200	0.0037	1.01

CE15	40	0.00541	3650	133000	7.0×10^7	0.0088	1.72	39800	50550	0.0037	0.99

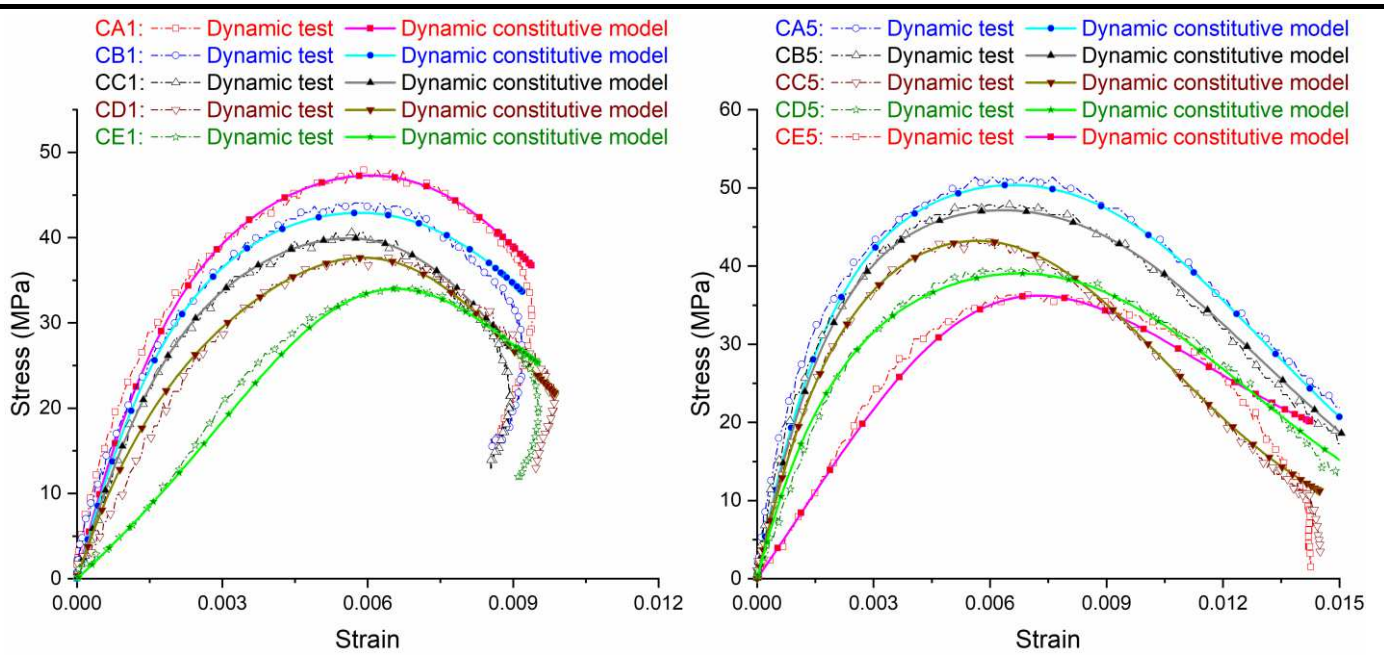

(a) Strain rate at 86±5s^{-1} (b) Strain rate at 104±5s^{-1}

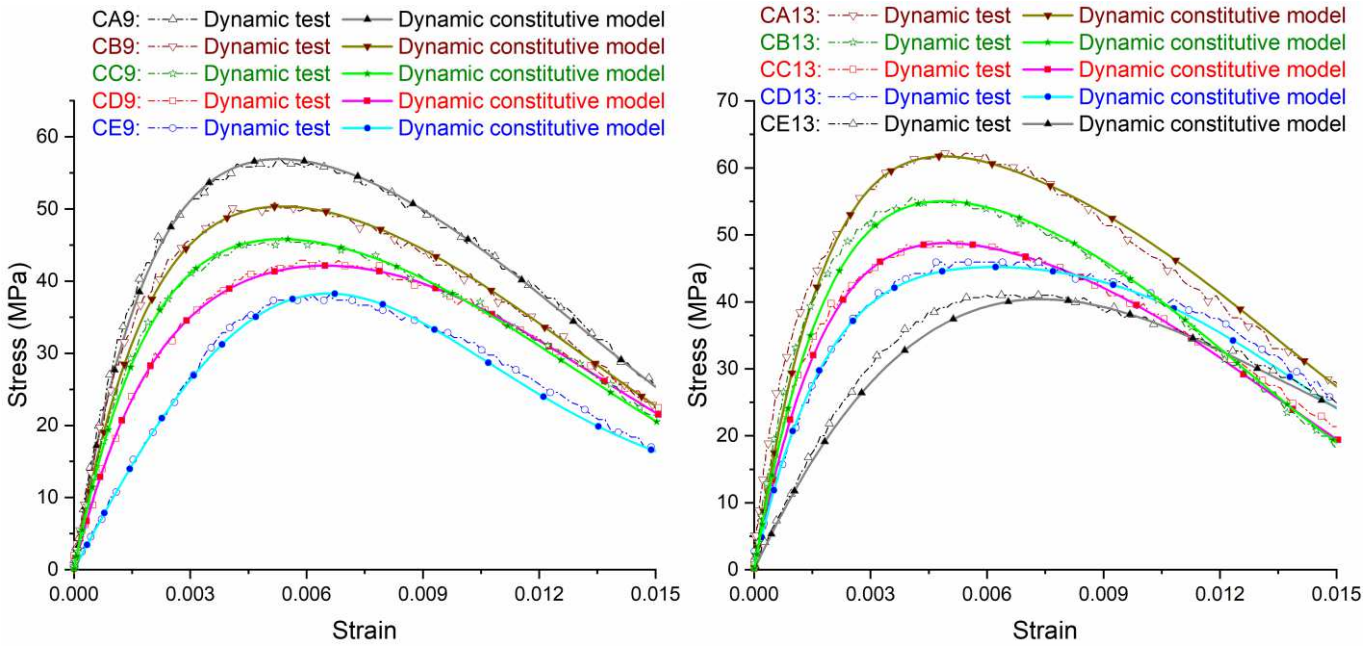

(c) Strain rate at 125±5s^{-1} (d) Strain rate at 152±5s^{-1}

Fig. 8 Comparison of water-saturated sandstone test curves and dynamic constitutive model curves

It should be noted that although the constitutive model involves many parameters, the form is simple. It can be seen from Table 3 that m_0 and m_2 have no specific rules, and their values range from 1.45 to 2.97 and 0.98 to 1.29, respectively. Under the same strain rate, the values of β and γ_0 of water-saturated sandstone after different freeze-thaw cycles are relatively close. In addition to the CE group, the values of E_0, α, E_2, and γ_2 in CA, CB, CC, and CD groups were also close. Under the same number of freeze-thaw cycles, except for the CE group, E_0, α, β, γ_0, and E_2 of water-saturated sandstone show obvious change rules with the increase of strain rate, and γ_2 is stable at about 0.0040. Therefore, except for the CE group with excessive freeze-thaw cycles, the dynamic stress-strain relationship of water-saturated sandstone under a

certain number of freeze-thaw cycles can be used to predict its dynamic mechanical behavior under different strain rates by using the established model. The abnormal parameters of the CE group are mainly due to the neglect of the low-frequency Maxwell model in the model establishment; when the number of freeze-thaw cycles is too large, the meso-damage of sandstone is serious, and the relaxation response of the low-frequency Maxwell model cannot be ignored, which leads to the deviation of the model parameters.

It can be seen from Fig. 9 that the theoretical curve of the model is highly consistent with the experimental stress-strain curve of frozen sandstone, and the fitting accuracy is higher than that of water-saturated sandstone, which indicates that the established model can accurately characterize the dynamic compression mechanical properties of frozen sandstone after cyclic freeze-thaw.

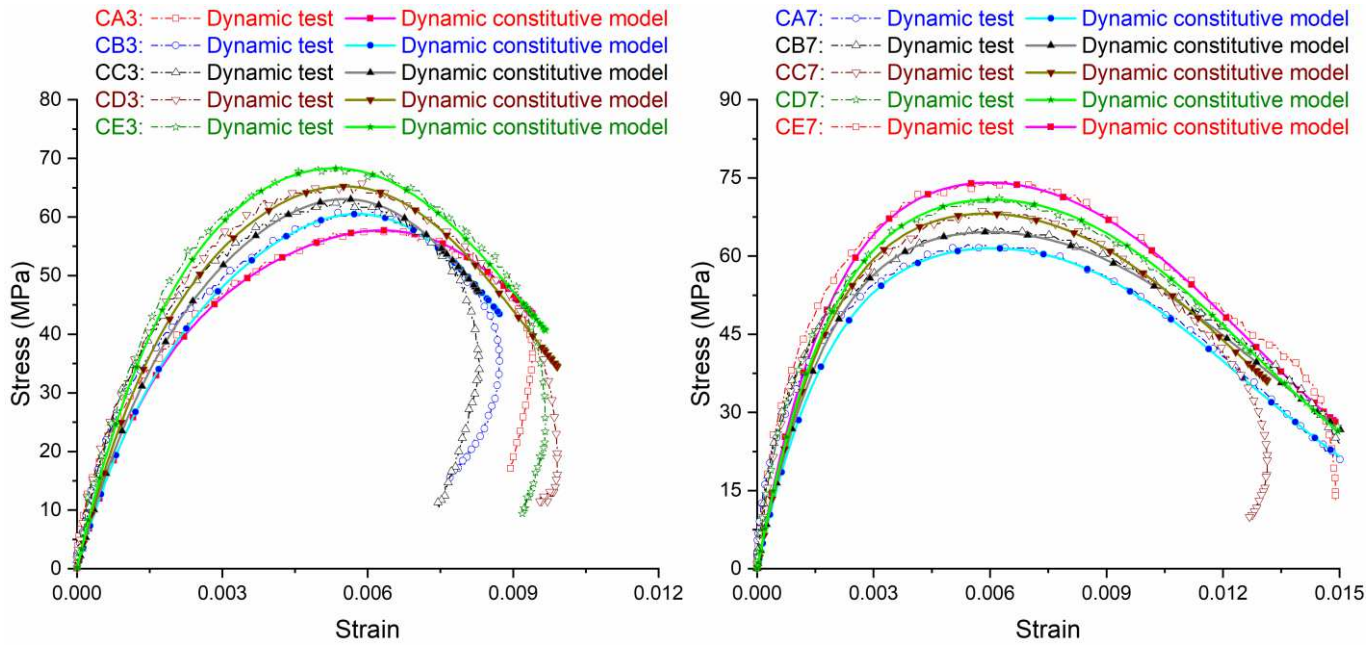

(a) Strain rate at 94±5s^{-1}

(b) Strain rate at 111±5s^{-1}

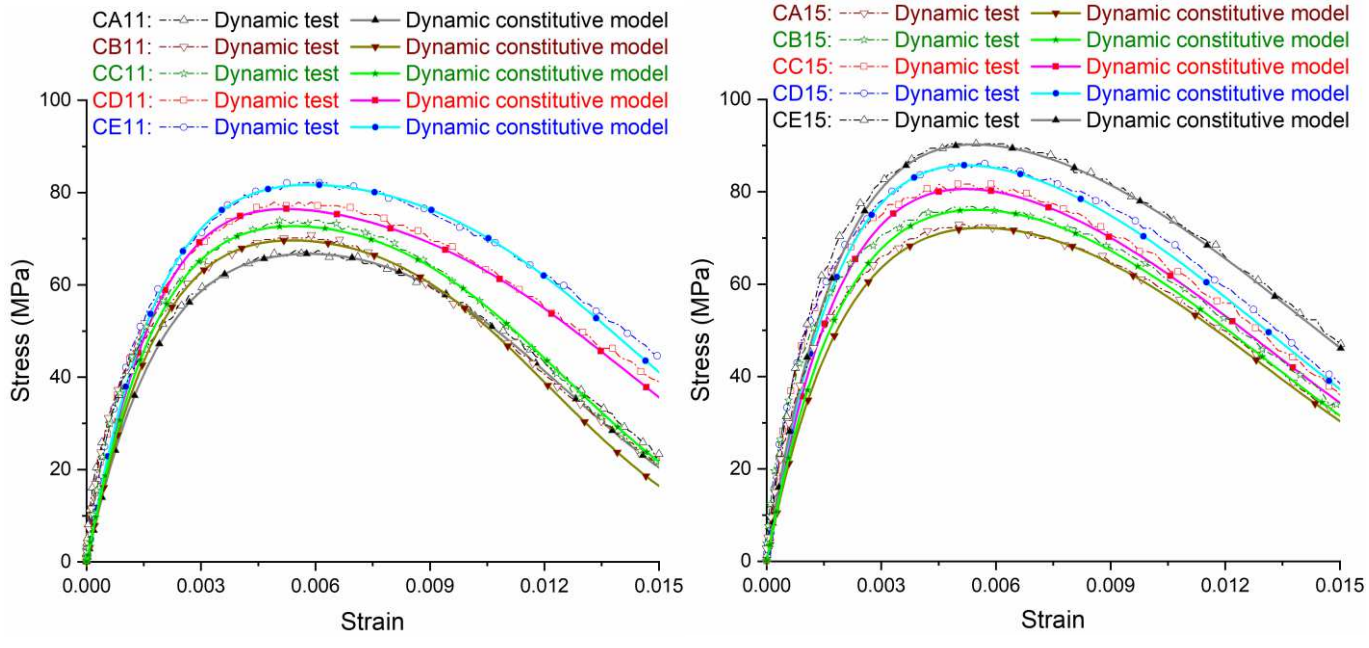

(c) Strain rate at 134±5s^{-1}

(d) Strain rate at 160±5s^{-1}

Fig. 9 Comparison of frozen sandstone test curves and dynamic constitutive model curves

For the frozen sandstone, it can be seen from table 3 that m_0 and m_2 have no specific rules, and their values range from 1.72 to 1.98 and 0.98 to 1.18, respectively, which are more concentrated than those of the water-saturated group. Under the same strain rate, the values of E_0, α, β, γ_0, E_2, and γ_2 of frozen sandstone after different freeze-thaw cycles are relatively close. Under the same number of freeze-thaw cycles, the above parameters show obvious change rules with the increase of strain rate, and γ_2 is stable at about 0.0037. Therefore, it can be considered that the dynamic stress-strain relationship of frozen sandstone under a certain number of freeze-thaw cycles is known, and the dynamic stress-strain relationship of frozen sandstone under different strain rates can be predicted by this dynamic constitutive model. Among them, compared with the CE-water-saturated group, there is no special case in the parameters of the CE-frozen group. It is speculated that the low-frequency Maxwell body strain response in the Z-W-T constitutive model will not affect the dynamic test results of the frozen sandstone, so it can be ignored.

4.2 Analysis of the effects of the parameters on the dynamic constitutive model

In order to reveal the influence law of each parameter on the dynamic damage constitutive model and further clarify the physical significance of the parameters, the specimen CC9 (water-saturated sandstone, 20 freeze-thaw cycles, 0.6 MPa impact pressure) and specimen CC11 (frozen sandstone, 20 freeze-thaw cycles, 0.6 MPa impact pressure) were selected as the research objects, and the control variable method was used to carry out the parameter sensitivity analysis. That is, only one parameter is changed at a time, and other parameters are kept constant, to study the influence of the change of each parameter on the stress-strain curve of the model.

Fig. 10 shows the effect of dynamic constitutive model parameters E_0 and E_2 on the curve of proposed dynamic constitutive model. It can be seen that the elastic constant E_0 (the elastic constant of the nonlinear elastic equilibrium response) E_2 (the elastic modulus of the high-frequency Maxwell model) have a significant influence on the slope of the linear elastic stage before the peak of the stress-strain curve, and then affect the elastic deformation, peak strength and post-peak failure characteristics of sandstone. The peak strength of sandstone is positively correlated with E_0 and E_2, and the connection line of the peak points under different parameter values is an approximately straight line. Compared with the water-saturated specimen CC9, the change of E_0 and E_2 of the frozen specimen CC11 has a greater influence on the strain rate corresponding to the peak strength; the slope of the peak point connection line of CC11 is smaller than that of CC9, which means that the peak strain changes more when reaching the same peak strength. In addition, the influence rate of E_2 on the peak strength is lower than that of E_0, which indicates that a larger change of E_2 is needed to produce the same influence on the peak strength of sandstone as E_0.

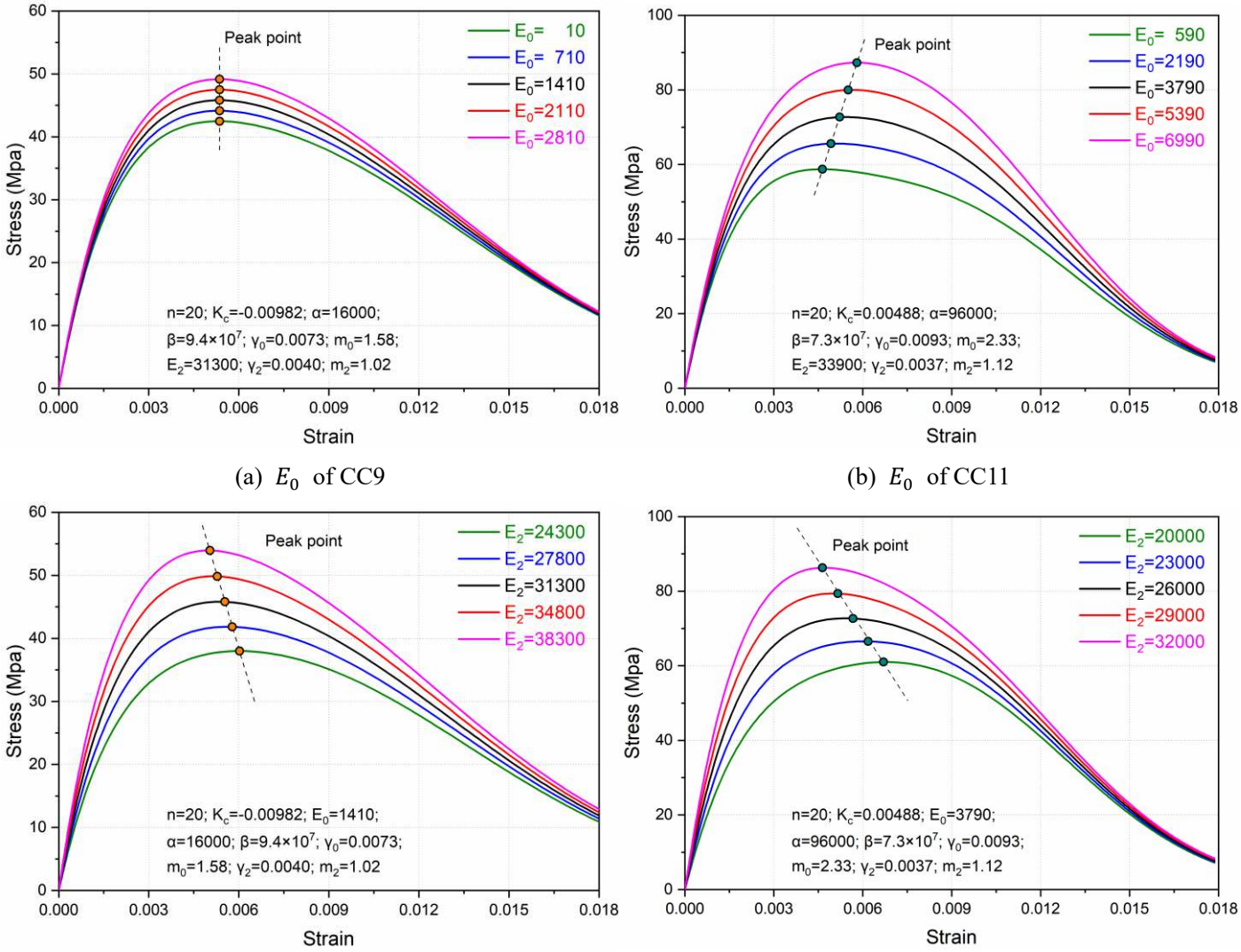

(a) E_0 of CC9 (b) E_0 of CC11

(c) E_2 of CC9 (d) E_2 of CC11

Fig. 10 The effect of dynamic constitutive model parameters: E_0 and E_2

Fig. 11 shows the influence of model parameters α and β on the curve of proposed dynamic constitutive model. It can be seen that the elastic constant α and β corresponding to the stress of the nonlinear elastic equilibrium response can control the trend of the nonlinear elastic section before the peak point, and then affect the elastic deformation, peak strength, and post-peak characteristics of sandstone. Compared with E_0 and E_2, the values of α and β have little effect on the slope of the first half before the peak point. The peak strength is positively correlated with α and β, and the connection of peak points can be approximated as a concave curve. Compared with the water-saturated specimen CC9, the α and β of CC11 have a greater effect on the strain rate corresponding to the peak strength. The slope change rate of the connection line between α and β of CC11 is smaller than that of CC9, and the depression degree of the connection line is slightly larger than that of CC9. In addition, the influence rate of α value on the peak strength is greater than that of β, which shows that the β value needs to change more greatly to have a similar influence on the shape of the stress-strain curve of the dynamic constitutive model.

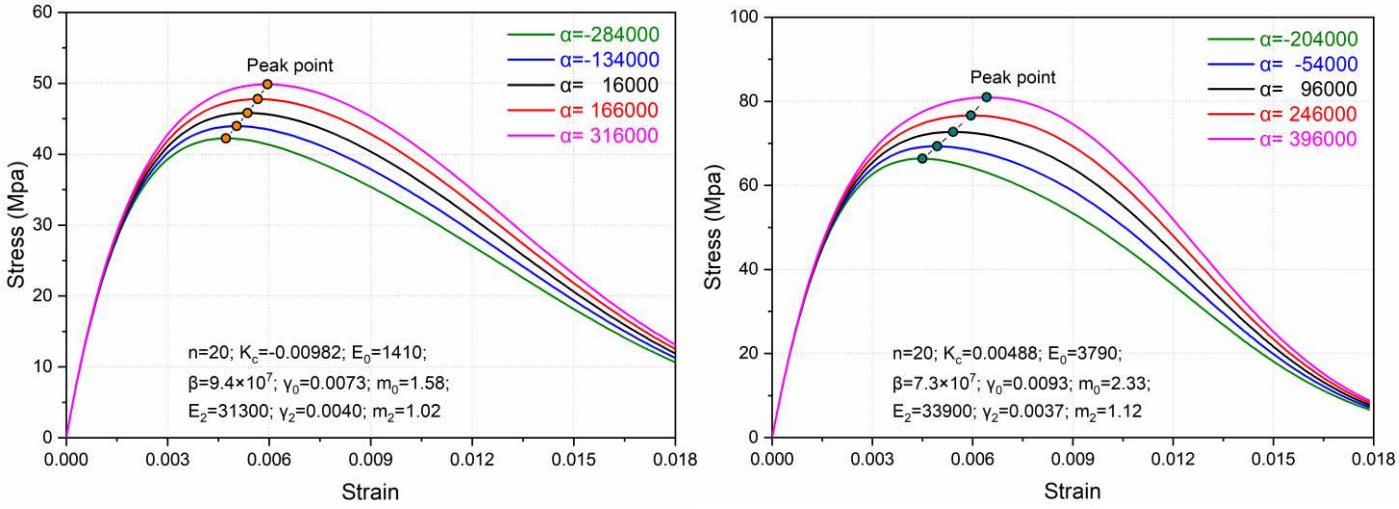

(a) α of CC9 (b) α of CC11

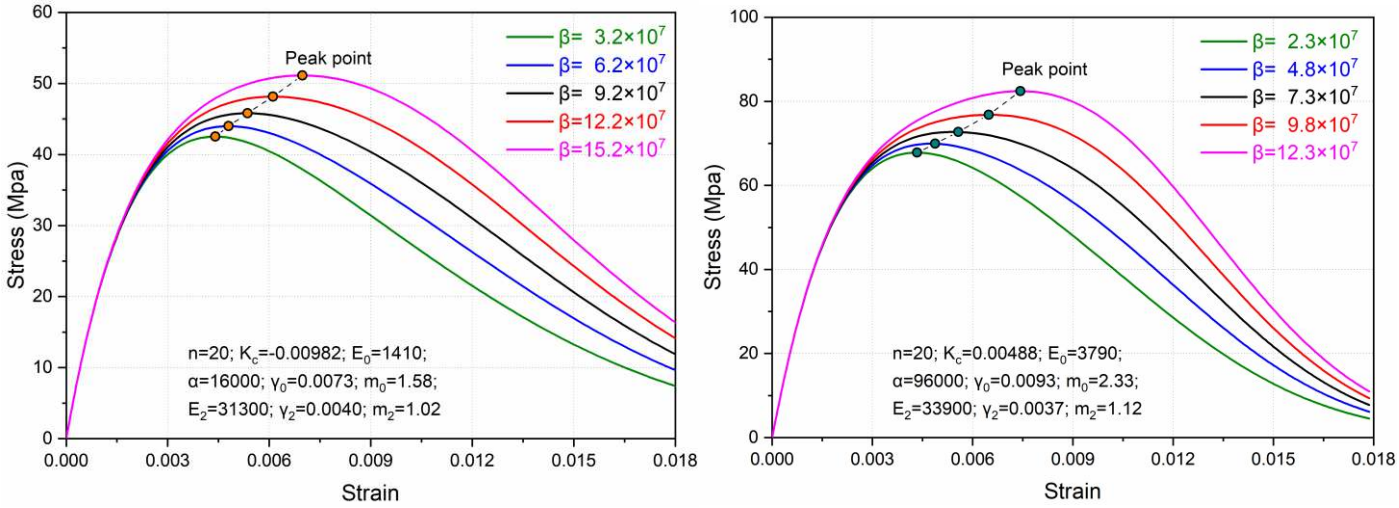

(c) β of CC9 (d) β of CC11

Fig. 11 The effect of dynamic constitutive model parameters: α and β

Fig. 12 shows the influence of model parameters γ_0 and γ_2 on the curve of proposed dynamic constitutive model. It can be seen from the figure that γ_0 and γ_2 mainly affect the viscous and plastic characteristics, and then affect the elastic deformation, peak strength, and post-peak characteristics of sandstone. As shown in Figs. 12a and 12b, compared with α and β, the value of γ_0 and γ_2 have little effect on the slope of the first half before the peak. When the γ_0 value changes, the peak strength point of the sandstone is delayed, and the peak point connection line is a curve that is first convex and then concave. When the γ_0 increases to a certain extent, the plastic characteristics of sandstone will be significantly strengthened, which is manifested as another straight line with a stable slope after the linear elastic section of the dynamic stress-strain curve until the peak strength is reached. The occurrence of the plastic strengthening stage also leads to the concave curve trend in the second half of the peak point connection line. As shown in Figs. 12c and 12d, the peak strength of sandstone is positively correlated with the γ_2, and the peak point connection line can be approximated as a concave curve, which is similar to α and β. The difference is that the γ_2 has a great influence on the peak strength, which is more obvious when the value is small. Compared

with CC9, the γ_2 value of CC11 is smaller, and the slope of the curve near the peak point is gentler, showing an oblique platform. When the γ_2 increases, the platform near the peak point of the stress-strain curve becomes less obvious.

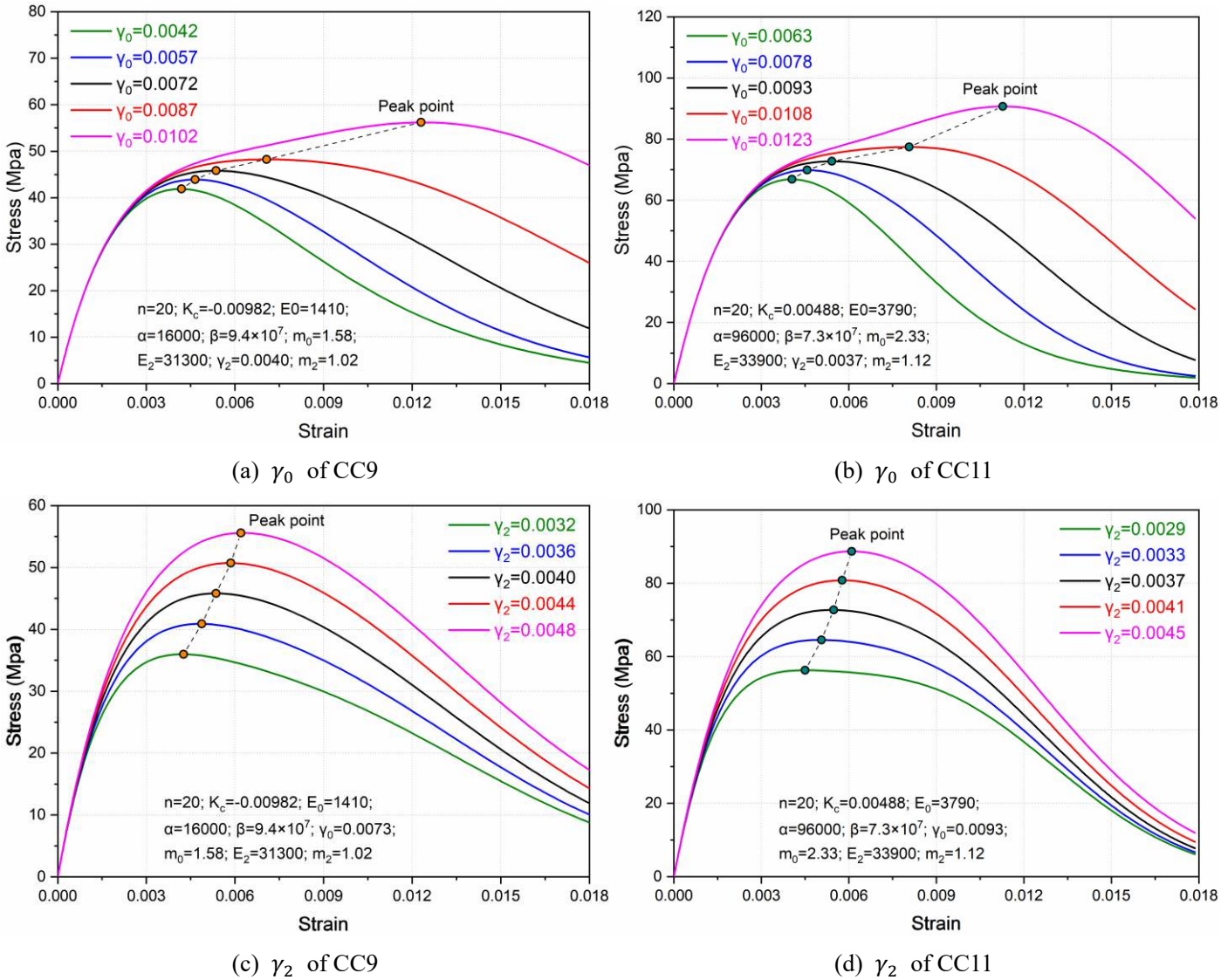

(a) γ_0 of CC9 (b) γ_0 of CC11

(c) γ_2 of CC9 (d) γ_2 of CC11

Fig. 12 The effect of dynamic constitutive model parameters: γ_0 and γ_2

Fig. 13 shows the influence of model parameters m_0 and m_2 on the curve of proposed dynamic constitutive model. It can be seen from the figure that m_0 and m_2 will affect the overall change characteristics of the stress-strain curve. When the m_0 and m_2 changes, the stress-strain curve intersects at a point after the peak point: Curve intersection. For CC9 and CC11, when the m_0 increases, the strength before the Curve intersection increases, and the strength after the Curve intersection decreases. The peak point connection line is shown in Figs.13a and 13b. The increase of m_0 leads to the advance of the peak point of CC9, resulting in the delay of the peak point of CC11. In addition, the effect of m_0 on CC9 was also significantly lower than that of CC11. When the m_2 increases, the peak point connection line is the concave curve shown in Figs. 13c and 13d, which is more obvious than the peak point connection line when the m_0 increases. For CC9 and CC11, when the m_2 increases, the strength before the Curve intersection increases,

and the strength after the Curve intersection decreases, which is the same as the influence of m_0. With the increase of m_2, the peak point of sandstone is advanced, and after exceeding a certain threshold, the peak point changes from after the Curve intersection to before the Curve intersection, which is a significant difference from m_0.

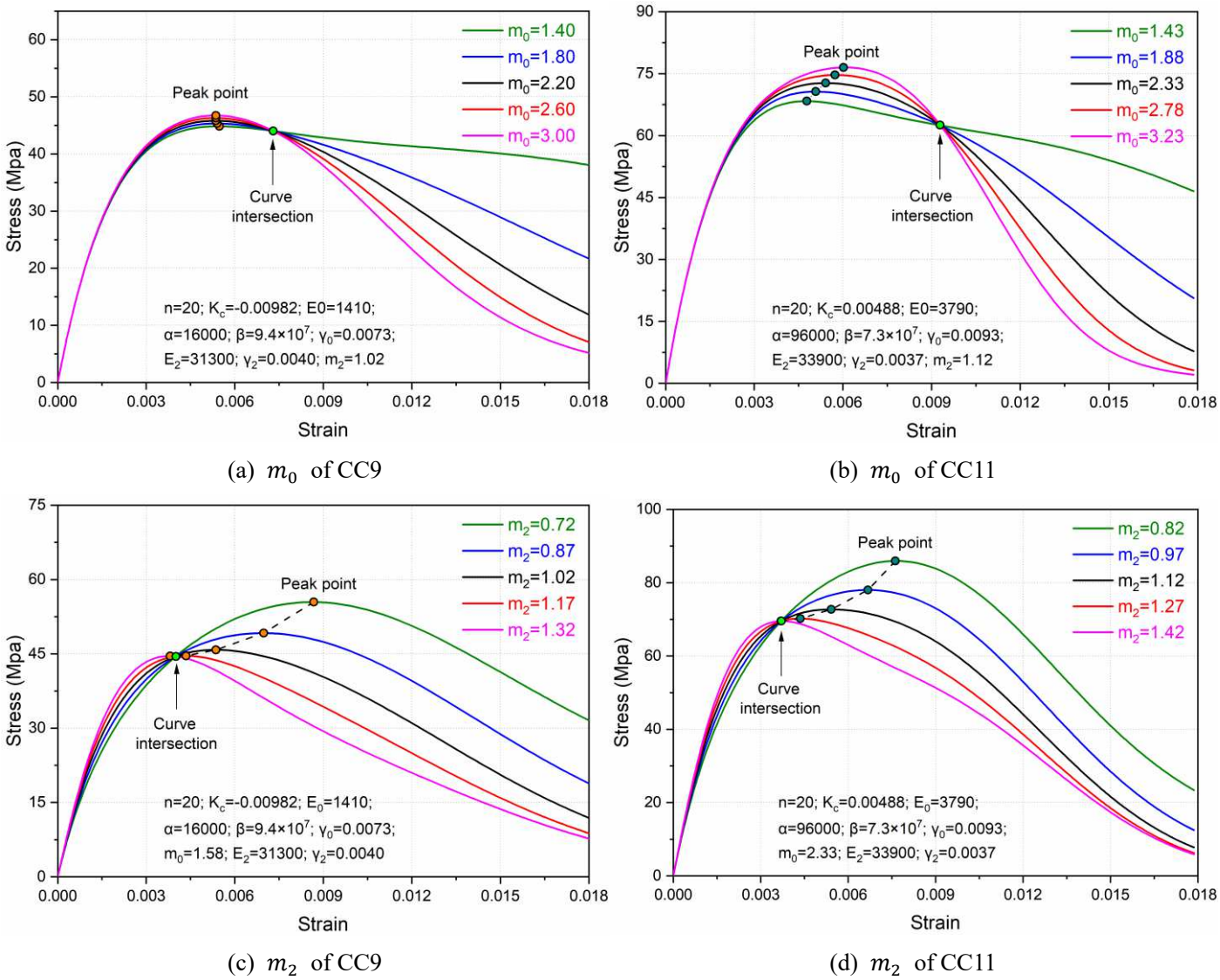

(a) m_0 of CC9 (b) m_0 of CC11

(c) m_2 of CC9 (d) m_2 of CC11

Fig. 13 The effect of dynamic constitutive model parameters: m_0 and m_2

Fig. 14 shows the influence of model parameter *n* on the curve of proposed dynamic constitutive model. It can be seen from the figure that *n* only controls the strength characteristics. For the water-saturated specimen CC9, the peak strength decreases with the increase of *n* value; for the frozen specimen CC11, the peak strength increases with the increase of *n* value, and the curve change is directly manifested as the longitudinal tension of the stress-strain curve. In addition, since the calculation of K_c is obtained by Eq. (23), the influence of K_c on the dynamic constitutive model is not studied.

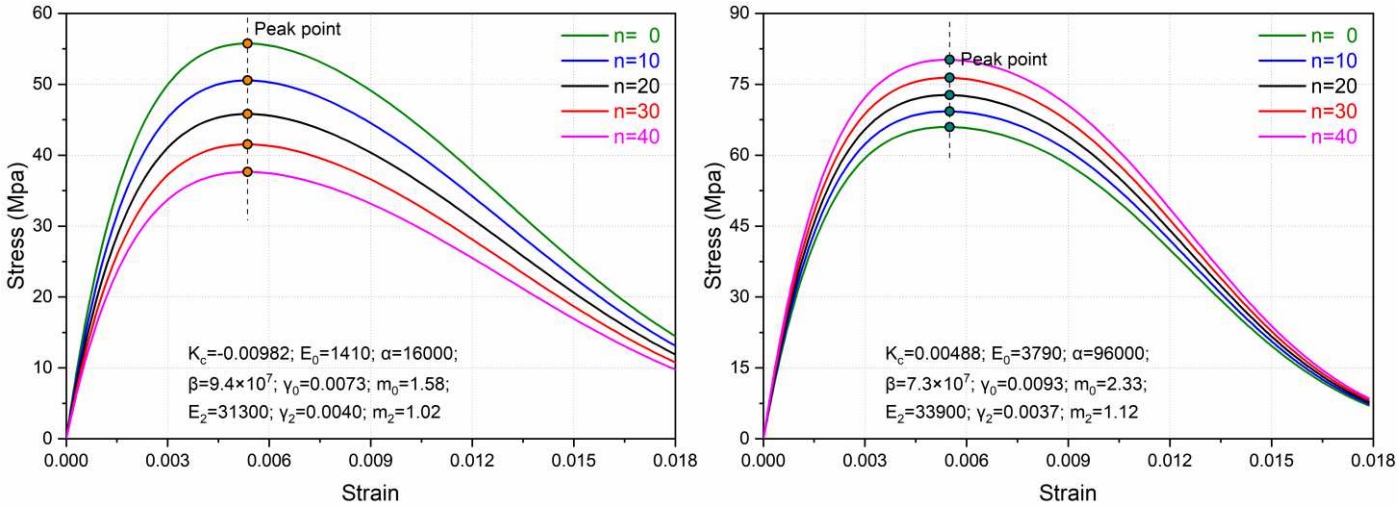

(c) n of CC9 (d) n of CC11

Fig. 14 The effect of dynamic constitutive model parameters: n

5 Conclusion

In this study, dynamic compression tests were carried out on sandstone specimens after 0, 10, 20, 30 and 40 freeze-thaw cycles by using modified SHPB, and a dynamic damage constitutive model of freeze-thawed sandstone considering initial meso-damage, freeze-thaw cycle times and test states was established based on the Z-W-T viscoelastic constitutive model. The model was verified by experimental data, and the parameter sensitivity analysis was carried out. The main conclusions are as follows:

(1) The model parameters m_0 and m_2 have no specific rules, but there is a fixed value range. The value range of m_0 and m_2 for frozen sandstone is more concentrated than that of saturated sandstone. Under the same strain rate, except for the CE group, the values of E_0, α, β, γ_0, E_2, and γ_2 of WSS and FS after different freeze-thaw cycles are relatively close. Under the same number of freeze-thaw cycles, E_0, α, β, γ_0, and E_2 of WSS and FS have obvious laws with the change of strain rate. Therefore, except for the CE group, it can be considered that the dynamic stress-strain relationship of WSS and FS under a certain number of freeze-thaw cycles is known, and that the dynamic stress-strain relationship of WSS and FS under different strain rates can be predicted by this dynamic constitutive model.

(2) According to the sensitivity analysis of the model parameters, it can be seen that E_0 and E_2 can control the slope of the linear elastic section before the peak point, and α and β can control the trend of the nonlinear elastic section before the peak point, which affects the elastic deformation, peak strength, and post-peak characteristics of frozen-thawed sandstone. Under the same conditions, the influence rate of E_2 on the peak strength is smaller than that of E_0, the influence rate of α value on the peak strength is greater than that of β. In addition, compared with the water-saturated specimen CC9, the E_0, E_2, α, and β of frozen specimen CC11 have a greater effect on the strain rate corresponding to the peak strength.

(3) The Weibull distribution parameters γ_0 and γ_2 mainly affect viscous and plastic characteristics.

When the γ_0 increases to a certain extent, the plastic characteristics of sandstone will be significantly strengthened. The effect of γ_2 on peak strength is similar to that of α and β, but when the γ_2 of frozen specimen CC11 is small, the slope of the curve near the peak point is gentler, showing an oblique platform.

(4) The Weibull distribution parameters m_0 and m_2 will affect the overall change characteristics of the stress-strain curve. When the m_0 and m_2 changes, the stress-strain curve intersects at a point after the peak point: Curve intersection. when the m_0 and m_2 increases, the strength before the Curve intersection increases, and the strength after the Curve intersection decreases. It is worth noting that with the increase of m_2, the peak point of sandstone is advanced, and after exceeding a certain threshold, the peak point changes from after the Curve intersection to before the Curve intersection, which is a significant difference from m_0.

6 Funding

This Paper supported by the National Natural Science Foundation of China(52574131).

7 References

Bruning T, Karakus M, Nguyen GD and Goodchild D (2019) An experimental and theoretical stress-strain-damage correlation procedure for constitutive modelling of granite. International Journal of Rock Mechanics and Mining Sciences 116: 1-12. doi: 10.1016/j.ijrmms.2019.03.003

Chen Y, Lin H and Cao R (2022) Damage constitutive model considering nonlinear fracture closure of rock under freezing–thawing cycles. Environmental Earth Sciences 82. doi: 10.1007/s12665-022-10695-0

Dai F, Huang S, Xia K and Tan Z (2010) Some fundamental issues in dynamic compression and tension tests of rocks using Split Hopkinson Pressure Bar. Rock Mechanics and Rock Engineering 43: 657-666. doi: 10.1007/s00603-010-0091-8

Fang W, Jiang N and Luo X (2019) Establishment of damage statistical constitutive model of loaded rock and method for determining its parameters under freeze-thaw condition. Cold Regions Science and Technology 160: 31-38. doi: 10.1016/j.coldregions.2019.01.004

Gao F, Li C, Xiong X, Zhang Y and Zhou K (2022) Dynamic behaviors of water-saturated and frozen sandstone subjected to freeze-thaw cycles. Journal of Rock Mechanics and Geotechnical Engineering. doi: 10.1016/j.jrmge.2022.11.007

Gao F, Xiong X, Xu C and Zhou K (2021) Mechanical property deterioration characteristics and a new constitutive model for rocks subjected to freeze-thaw weathering process. International Journal of Rock Mechanics and Mining Sciences 140. doi: 10.1016/j.ijrmms.2021.104642

Huang S, Liu Q, Cheng A and Liu Y (2018) A statistical damage constitutive model under freeze-thaw and loading for rock and its engineering application. Cold Regions Science and Technology 145: 142-150. doi: 10.1016/j.coldregions.2017.10.015

Huang X, Pang J and Zou J (2022) Study on the effect of dry–wet cycles on dynamic mechanical properties of sandstone under sulfuric acid solution. Rock Mechanics and Rock Engineering 55: 1253-1269. doi: 10.1007/s00603-021-02729-z

Jiang W, Lai Y, Yu F, Ma Q and Jiang H (2023) Mechanical properties investigation and damage constitutive models of red sandstone subjected to freeze-thaw cycles. Cold Regions Science and Technology 207. doi: 10.1016/j.coldregions.2023.103776

Ke B, Zhou K, Xu C, Deng H, Li J and Bin F (2018) Dynamic mechanical property deterioration model of sandstone caused by freeze–thaw weathering. Rock Mechanics and Rock Engineering 51: 2791-2804. doi: 10.1007/s00603-018-1495-0

Lemaitre J (1996) A course on damage mechanics. Springer-Verlag Berlin Heidelberg,

Li X, Cao W-G and Su Y-H (2012) A statistical damage constitutive model for softening behavior of rocks. Engineering Geology 143-144: 1-17. doi: 10.1016/j.enggeo.2012.05.005

Li X, Zhou Z, Lok T-S, Hong L and Yin T (2008) Innovative testing technique of rock subjected to coupled static and dynamic loads. International Journal of Rock Mechanics and Mining Sciences 45: 739-748. doi: 10.1016/j.ijrmms.2007.08.013

Li XB, Lok TS and Zhao J (2004) Dynamic characteristics of granite subjected to intermediate loading rate. Rock Mechanics and Rock Engineering 38: 21-39. doi: 10.1007/s00603-004-0030-7

Liang X, Tang S, Tang Ca, Hu L and Chen F (2022) Influence of water on the mechanical properties and failure behaviors of sandstone under triaxial compression. Rock Mechanics and Rock Engineering 56: 1131-1162. doi: 10.1007/s00603-022-03121-1

Lin H, Liang L, Chen Y, Cao R and Guo W-y (2021) A damage constitutive model of rock subjected to freeze-thaw cycles based on lognormal distribution. Advances in Civil Engineering 2021: 1-8. doi: 10.1155/2021/6658915

Lin Y, Zhou K, Li J, Ke B and Gao R (2019) Weakening laws of mechanical properties of sandstone under the effect of chemical corrosion. Rock Mechanics and Rock Engineering 53: 1857-1877. doi: 10.1007/s00603-019-01998-z

Liu H, Yuan X and Xie T (2019) A damage model for frost heaving pressure in circular rock tunnel under freezing-thawing cycles. Tunnelling and Underground Space Technology 83: 401-408. doi: 10.1016/j.tust.2018.10.012

Liu H, Zhang X, Yan X and Wang Y (2021) A damage constitutive model for a rock under compression after freeze-thaw cycles based on the micromechanics. Geofluids 2021: 1-11. doi: 10.1155/2021/3177464

564 Liu X, Liu Y, Dai F and Yan Z (2022) Tensile mechanical behavior and fracture characteristics of sandstone
565 exposed to freeze-thaw treatment and dynamic loading. International Journal of Mechanical Sciences
566 226. doi: 10.1016/j.ijmecsci.2022.107405
567 Lu Y, Li X and Chan A (2019) Damage constitutive model of single flaw sandstone under freeze-thaw and
568 load. Cold Regions Science and Technology 159: 20-28. doi: 10.1016/j.coldregions.2018.11.017
569 Ma D, Ma Q and Yuan P (2017) Shpb tests and dynamic constitutive model of artificial frozen sandy clay
570 under confining pressure and temperature state. Cold Regions Science and Technology 136: 37-43. doi:
571 10.1016/j.coldregions.2017.01.004
572 Ma H, Song Y, Chen S, Yin D, Zheng J, Shen F, Li X and Ma Q (2021) Experimental investigation on the
573 mechanical behavior and damage evolution mechanism of water-immersed gypsum rock. Rock
574 Mechanics and Rock Engineering 54: 4929-4948. doi: 10.1007/s00603-021-02548-2
575 Meng X, Zhang H and Liu X (2021) Rock damage constitutive model based on the modified logistic equation
576 under freeze–thaw and load conditions. Journal of Cold Regions Engineering 35. doi:
577 10.1061/(asce)cr.1943-5495.0000268
578 Miao S, Pan P-Z, Zhao X, Shao C and Yu P (2020) Experimental study on damage and fracture characteristics
579 of beishan granite subjected to high-temperature treatment with dic and ae techniques. Rock Mechanics
580 and Rock Engineering 54: 721-743. doi: 10.1007/s00603-020-02271-4
581 Momeni A, Abdilor Y, Khanlari GR, Heidari M and Sepahi AA (2015) The effect of freeze–thaw cycles on
582 physical and mechanical properties of granitoid hard rocks. Bulletin of Engineering Geology and the
583 Environment 75: 1649-1656. doi: 10.1007/s10064-015-0787-9
584 Park J, Hyun C-U and Park H-D (2014) Changes in microstructure and physical properties of rocks caused by
585 artificial freeze–thaw action. Bulletin of Engineering Geology and the Environment 74: 555-565. doi:
586 10.1007/s10064-014-0630-8
587 Qu D, Li D, Li X, Luo Y and Xu K (2018) Damage evolution mechanism and constitutive model of freeze-
588 thaw yellow sandstone in acidic environment. Cold Regions Science and Technology 155: 174-183. doi:
589 10.1016/j.coldregions.2018.07.012
590 Rong G, Sha S, Li B, Chen Z and Zhang Z (2021) Experimental investigation on physical and mechanical
591 properties of granite subjected to cyclic heating and liquid nitrogen cooling. Rock Mechanics and Rock
592 Engineering 54: 2383-2403. doi: 10.1007/s00603-021-02390-6
593 Shen P, Tang H, Ning Y and Xia D (2019) A damage mechanics based on the constitutive model for strain-
594 softening rocks. Engineering Fracture Mechanics 216. doi: 10.1016/j.engfracmech.2019.106521

595 Shi L, Liu Y, Meng X, Zhang H and Dede T (2021) Study on mechanical properties and damage characteristics
596 of red sandstone under freeze-thaw and load. Advances in Civil Engineering 2021: 1-13. doi:
597 10.1155/2021/8867489
598 Tang C (1997) Numerical simulation of progressive failure and associated seismicity. International Journal of
599 Rock Mechanics and Mining Sciences 34: 249-261.
600 Török Á, Ficsor A, Davarpanah M and Vásárhelyi B (2018) Comparison of mechanical properties of dry,
601 saturated and frozen porous rocks. Iaeg/aeg annual meeting proceedings, san francisco, california,
602 2018—volume 6, Springer International Publishing, pp 113-118
603 Ulusary R (2014) The isrm suggested methods for rock characterization, testing and monitoring: 2007–2014.
604 Springer International Publishing, Switzerland
605 Wang J, Zhang Q, Song Z, Zhang Y and Liu X (2021) Mechanical properties and damage constitutive model
606 for uniaxial compression of salt rock at different loading rates. International Journal of Damage
607 Mechanics 30: 739-763. doi: 10.1177/1056789520983868
608 Wang T, Jia H, Sun Q, Lu T, Luo T and Shen Y (2023) Failure of frozen sandstone under uniaxial compression
609 with interpretation of pressure melting of pore ice from electrical resistance. Journal of Geotechnical and
610 Geoenvironmental Engineering 149. doi: 10.1061/jggefk.Gteng-11025
611 Wang T, Sun Q, Jia H, Ren J and Luo T (2021) Linking the mechanical properties of frozen sandstone to
612 phase composition of pore water measured by lf-nmr at subzero temperatures. Bulletin of Engineering
613 Geology and the Environment 80: 4501-4513. doi: 10.1007/s10064-021-02224-3
614 Wang Y, Zhu C, He M, Wang X and Le H (2022) Macro-meso dynamic fracture behaviors of xinjiang marble
615 exposed to freeze thaw and frequent impact disturbance loads: A lab-scale testing. Geomechanics and
616 Geophysics for Geo-Energy and Geo-Resources 8. doi: 10.1007/s40948-022-00472-5
617 Wang Z, Zhu Z and Zhu S (2019) Thermo-mechanical-water migration coupled plastic constitutive model of
618 rock subjected to freeze-thaw. Cold Regions Science and Technology 161: 71-80. doi:
619 10.1016/j.coldregions.2019.03.001
620 Wang ZL, Shi H and Wang JG (2018) Mechanical behavior and damage constitutive model of granite under
621 coupling of temperature and dynamic loading. Rock Mechanics and Rock Engineering 51: 3045-3059.
622 doi: 10.1007/s00603-018-1523-0
623 Weng L, Wu Z and Liu Q (2020) Dynamic mechanical properties of dry and water-saturated siltstones under
624 sub-zero temperatures. Rock Mechanics and Rock Engineering 53: 4381-4401. doi: 10.1007/s00603-
625 019-02039-5

626 Zhang F, Zhu Z, Fu T and Jia J (2020) Damage mechanism and dynamic constitutive model of frozen soil
627 under uniaxial impact loading. Mechanics of Materials 140. doi: 10.1016/j.mechmat.2019.103217
628 Zhang H, Meng X and Liu X (2021) Establishment of constitutive model and analysis of damage
629 characteristics of frozen-thawed rock under load. Arabian Journal of Geosciences 14. doi:
630 10.1007/s12517-021-07598-y
631 Zhang H, Meng X and Yang G (2020) A study on mechanical properties and damage model of rock subjected
632 to freeze-thaw cycles and confining pressure. Cold Regions Science and Technology 174. doi:
633 10.1016/j.coldregions.2020.103056
634 Zhou S, Jiang N, Luo X, Fang W and He X (2020) Uniaxial compression fractal damage constitutive model
635 of rock subjected to freezing and thawing. Periodica Polytechnica Civil Engineering. doi:
636 10.3311/PPci.15313